Nonlinear Dyn (2017) 90:1501–1517
DOI 10.1007/s11071-017-3792-7

REVIEW

Aeroelastic effect on modal interaction and dynamic behavior of acoustically excited metallic panels

Xiao-Chen Wang · Zhi-Chun Yang · Ying-Song Gu · Wei Wang · Zhao-Lin Chen

Received: 8 November 2016 / Accepted: 5 September 2017 / Published online: 15 September 2017

Abstract This paper details the study of the aeroelastic effect on modal interaction and dynamic behavior of acoustically excited square metallic panels with fully clamped edges using finite element method. The first-order shear deformation plate theory and von Karman nonlinear strain–displacement relationships are employed to consider the structural geometric nonlinearity caused by large vibration deflections. Piston aerodynamic theory and Gaussian white noise are used to simulate the aerodynamic load and the acoustic load, respectively. Motion equations are derived by the principle of virtual work in the physical coordinates and then transformed into the truncated modal coordinates with reduced orders. Runge–Kutta method is employed to obtain the system response, and the modal interaction mechanism is quantitatively valued by the modal participation distribution. Results show that in the pre-/near-flutter regions, in addition to the dominant fundamental resonant mode, the first twin companion antisymmetric modes can be largely excited by the aeroelastic coupling mechanism; thus, aeroelastic modal participation distribution and the spectrum response can be altered, while the dynamic behavior still exhibits linear random vibrations. In the post-flutter region, the dominant flutter motion can be enriched by highly ordered odd order super-harmonic motion occurs due to 1:1 internal resonances. Correspondingly, the panel dynamic behavior changes from random vibration to highly ordered motions in the fashion of diffused limit-cycle oscillations (LCOs). However, this LCOs motion can be affected by the intensifying acoustic excitation through changing the aeroelastic modal interaction mechanism. Accompanied with these changes, the panel can experience various stochastic bifurcations.

Keywords Aeroelastic effect · Modal interaction · Panel flutter · 1:1 Internal resonance · Stochastic bifurcation

1 Introduction

Most skin panels of high-speed air vehicles or spacecrafts are simultaneously subjected to combined loads from boundary layer turbulence, engine noise, and mean flow fluctuations. With a longtime duration exposed to such extreme environment, panel sonic fatigue becomes a major concern to the high-speed vehicles [1]. To avoid an over-conservative design, there arises a need to accurately predict the vibration response of such panels in coupled multi-fields.

As a main source of panel sonic fatigue, the acoustic load, induced by boundary layer turbulence (may be combined with the engine noise in some specific regions), was approximated to be in the range of 130–170 dB [1]. To simulate the acoustic environment for

X.-C. Wang · Z.-C. Yang (✉) · Y.-S. Gu · W. Wang · Z.-L. Chen
School of Aeronautics, Northwestern Polytechnical University, Xi'an 710072, China
e-mail: yangzc@nwpu.edu.cn

X.-C. Wang
e-mail: wxc_npu@163.com

research, there exist three different approaches until the flight test data are available, namely (i) a random in time, uniform in space, prescribed acoustic load, (ii) semiempirical models [2], and (iii) computational fluid dynamics (CFD) [3]. As the first approach is simple to implement, and its spatial correlated characteristics can be reasonably neglected considering the smaller panel scale respect to its attached boundary layer, this approach has been widely adopted. Additionally, it is required to consider the mean flow fluctuating load due to the aeroelastic coupling mechanism [3]. This aerodynamic load can lead to the aeroelastic instability problem, i.e., panel flutter, which mainly deals with predicting the critical flow velocity and the corresponding frequencies (modes). Motivated by the need for a better understanding of the nonlinear vibration response of skin panels under such combined loads, many researchers have used different approaches to investigate this multi-physical problem. Most existed studies treated panel flutter as a pure dynamic instability problem with merely mean flow considered; however, some studies took the boundary layer influence into account. These studies should be motivated by the experimental studies, which indicated the importance of the boundary layer [4,5]. Then, Dowell [6] assumed a particular velocity profile with (1/7)th power velocity law to simulate the boundary layer and studied its influence. By using the laminar boundary layer model, Vasily [7] investigated the interaction of panel flutter with inviscid boundary layer in supersonic flow. Additionally, other researchers also investigated the boundary layer by using CFD method [8–10].

These studies focused on building a coupled model with both mean flow and boundary layer considered. To simplify this problem, the pressure perturbation from boundary layer or engine noise can be assumed as random acoustic excitation with specific spectrum [11]. Thus, a finite element formulation was presented for the response analysis of composite panels subjected to both the acoustic excitation and aerodynamic pressure [12]. The results suggested that both the acoustic and aerodynamic loads have to be considered in the post-flutter region from the perspective of deflections. Additionally, considering the thermal-induced membrane load, nonlinear aerothermoacoustic response of shape memory alloy hybrid composite panels was investigated, and the thermal-induced snap-through was observed merely based on the deflection time histories [13]. Then, a 2-DOF simple computational panel model based on a novel two-way coupling method was implemented to investigate the impact of flow induced load on the snap-through behavior of the acoustically excited, thermal buckled panels [3]. Results showed that the self-induced aerodynamic load can significantly affect the vibration response of panels under random acoustic load, while the random forced pressure can reduce the onset time of panel flutter. The above results were also mainly obtained from the system deflection time histories. To comprehensively investigated the interaction mechanism between the flutter motion and the forced response, a parametric study [14], based on a 2-DOF simple mechanical system, was implemented to investigate the effect of small periodic disturbances on the panel aeroelastic response. The results showed that the external disturbance force can induce a smooth transition prior to the flutter occurrence obtained from the linear panel flutter theory, and the frequency response can be altered. Recently, Wang [15] explored the aeroelastic effect on the aerothermoacoustic response of metallic panels from perspectives of both the spectrum response and the stochastic bifurcation characteristics using finite element method. Zhao [16] conducted a parametric study on supersonic flutter of composite panel in coupled multi-fields, where the significant influence of both the thermal and acoustic loading was confirmed.

Considering that the motion governing equations can be transformed into a set of aeroelastic coupled nonlinear Duffing oscillators driven by a wideband random excitation in physical nature, thus the system modal interaction mechanism can be affected by the frequency coalescence mechanism (panel flutter) and internal/external resonances. In addition to the well-known panel flutter, internal resonances exist when the structural eigenfrequencies are commensurable, or nearly so. However, an integer eigenfrequency ratio does form a necessary condition for internal resonance mechanism to exchange energy as the internal resonance presences depend on the geometry, nonlinearity, and system boundary conditions of the system [17]. In study [18], a 2-DOF panel aeroelastic system, with repeated eigenfrequencies and cubic nonlinearity to a principal parametric excitation, was treated as an one-to-one (1:1) internal resonances system and investigated. As more higher-order modes were not considered in this study, thus more complicated internal resonance mechanisms cannot be observed. In the studies using a two-degree-of-freedom airfoil model [19,20],

1:3, 1:2, and 1:1 internal resonances were investigated as the flow velocity increases. It was found that the presence of cubic nonlinear stiffness in the aeroelastic system can led to 1:3 internal resonances. Recently, the 1:3 internal resonances were observed in a nonlinear panel flutter system and treated as a cause of nonlinear panel flutter by using direct Naiver–Stokes (DNS) method [21,22]. Additionally, the system dynamic response can be complicated by the geometric nonlinearity due to large deflections with panel thickness level. This nonlinearity can not only prevent the panel from immediate flutter collapse, but also result in the nonlinear frequency–amplitude response (NFR). Accompanied with panel flutter, internal/external resonance mechanism, and nonlinear frequency–amplitude response, the dynamic response of panel will exhibit different stochastic bifurcations with varying parameters. These bifurcations indicate the changes in number, locations, shapes, and magnitudes of the peaks of the deflections probability density distribution [23]. Thus, the mean strain and vibratory strain of the panel can be significantly altered.

As noted by the above discussion, to better understand various aeroelastic behaviors of such panels, the modal interaction mechanism within this forced aeroelastic system should be highly emphasized. As an extension work of the previous work [15], the presented analysis emphasizes on how can the modal interaction mechanism be regulated by the aeroelastic effect and attempts to understand the balance relationship between the flutter motion and the external wideband random excitation figured out by works [12,15]. Without considering the variation of the panel modes (frequencies) due to thermal elevations, the motion equation is formulated by using finite elements method and virtual principle and is calculated by numerical integration method. In addition to the conventional behavior study, the varying frequencies of the updated aeroelastic system with changing flow dynamic pressures is presented, and the modal participation is presented to quantitatively investigate the modal interaction mechanism. Finally, the corresponding dynamic behaviors are analyzed.

2 Formulations and solution procedure

The multi-physical system in this study is schematically depicted in Fig. 1. It is shown that the mean flow passes over the upside surface of the acoustically excited, square metallic panel. The mean flow and the vibrating panel can build the traditional aeroelastic self-sustained system, while the uniformly distributed, random load is treated as a pure external excitation [15].

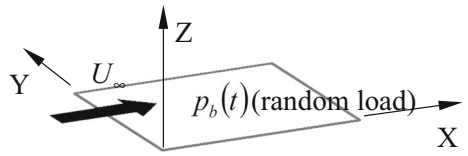

Fig. 1 Schematic diagram of acoustically excited skin panels in high-speed flow

Following with the presented detailed formulation [12,15], without considering the thermal-induced membrane load, the main formulation procedure is presented again in this section. By using the first- order deformation theory [23], the displacement fields of the panel can be expressed as:

$$\begin{cases} u(x, y, z) = u_0(x, y) + z\varphi_y(x, y) \\ v(x, y, z) = v_0(x, y) + z\varphi_x(x, y) \\ w(x, y, z) = w_0(x, y) \end{cases} \tag{1}$$

where $u(x, y, z)$, $v(x, y, z)$, and $w(x, y, z)$ denote the panel displacements along x, y, and z directions, respectively, and z is the transverse coordinate. $u_0(x, y)$, $v_0(x, y)$, and $w_0(x, y)$ denote three middle plane displacements along x, y, and z directions, respectively. φ_x and φ_y denote the rotations of the normal to the mid-surface respect to the x- and y-axes, respectively.

The nodal degrees-of-freedom vector of a Mindlin plate element (MIN3) is expressed as [12,15,25]:

$$\begin{aligned} [\![\boldsymbol{w}_b \ [\boldsymbol{\varphi}_x \ \boldsymbol{\varphi}_y]\!] \quad [\boldsymbol{u} \ \boldsymbol{v}]]^T &= \left[\begin{bmatrix} \boldsymbol{w}_b \\ \boldsymbol{w}_\varphi \end{bmatrix} \quad \boldsymbol{w}_m \right] = \begin{bmatrix} \boldsymbol{w}_B \\ \boldsymbol{w}_m \end{bmatrix} \\ &= \boldsymbol{w} \end{aligned} \tag{2}$$

where $[\boldsymbol{w}_B] = \begin{bmatrix} \boldsymbol{w}_b & \boldsymbol{w}_\varphi \end{bmatrix}^T$, $[\boldsymbol{w}_\varphi] = \begin{bmatrix} \boldsymbol{\varphi}_x & \boldsymbol{\varphi}_y \end{bmatrix}^T$, and $\boldsymbol{w}_b$ denotes the middle plane transverse displacement vector and φ_x and $\boldsymbol{\varphi}_y$ denote the rotations vectors of the normal to the mid-surface respect to the x- and y-axes, respectively. $\boldsymbol{w}_m$ denotes the membrane displacement vector. The relation between the element displacements and the nodal displacements can be expressed as [15, 25]:

$$\begin{cases} \boldsymbol{u}_0 = \boldsymbol{H}_{\mathrm{u}}\boldsymbol{w}_{\mathrm{m}} \\ \boldsymbol{v}_0 = \boldsymbol{H}_{\mathrm{v}}\boldsymbol{w}_{\mathrm{m}} \\ \boldsymbol{w}_0 = \boldsymbol{H}_{\mathrm{w}}\boldsymbol{w}_{\mathrm{b}} + \boldsymbol{H}_{\mathrm{w}\varphi}\boldsymbol{w}_{\varphi} \\ \boldsymbol{\varphi}_{\mathrm{x}} = \boldsymbol{H}_{\varphi\mathrm{x}}\boldsymbol{w}_{\varphi} \\ \boldsymbol{\varphi}_{\mathrm{y}} = \boldsymbol{H}_{\varphi\mathrm{y}}\boldsymbol{w}_{\varphi} \end{cases} \tag{3}$$

where $\boldsymbol{H}_{\mathrm{u}}$ and $\boldsymbol{H}_{\mathrm{v}}$ denote the in-plane displacement interpolation shape function matrices, $\boldsymbol{H}_{\mathrm{w}}$ denotes the transverse displacement interpolation shape function matrix, and $\boldsymbol{H}_{\mathrm{w}\varphi}$, $\boldsymbol{H}_{\varphi\mathrm{x}}$, and $\boldsymbol{H}_{\varphi\mathrm{y}}$ denote the rotation displacement interpolation shape function matrices [15,25]. Based on the von Karman theory, the in-plane strains and curvatures can be written as:

$$\boldsymbol{\varepsilon} = \boldsymbol{\varepsilon}_{\mathrm{m}} + \boldsymbol{\varepsilon}_{\mathrm{mb}} + z\boldsymbol{k} \tag{4}$$

where $\boldsymbol{\varepsilon}_{\mathrm{m}}$, $\boldsymbol{\varepsilon}_{\mathrm{mb}}$, and $z\boldsymbol{k}$ denote the linear membrane strain vector, the nonlinear membrane strain vector, and the bending strain vector, respectively. The stress–strain relations of a metallic panel are,

$$\begin{bmatrix} \boldsymbol{\sigma} \\ \boldsymbol{\tau} \end{bmatrix} = \begin{bmatrix} \begin{bmatrix} \sigma_{\mathrm{x}} \\ \sigma_{\mathrm{y}} \\ \tau_{\mathrm{xy}} \end{bmatrix} \\ \begin{bmatrix} \tau_{\mathrm{yz}} \\ \tau_{\mathrm{xz}} \end{bmatrix} \end{bmatrix}$$

$$= \begin{bmatrix} \frac{E}{1-v^2} & \frac{E}{1-v^2} & 0 & 0 & 0 \\ \frac{E}{1-v^2} & \frac{E}{1-v^2} & 0 & 0 & 0 \\ 0 & 0 & G & 0 & 0 \\ 0 & 0 & 0 & G & 0 \\ 0 & 0 & 0 & 0 & G \end{bmatrix} \begin{bmatrix} \begin{bmatrix} \varepsilon_{\mathrm{x}} \\ \varepsilon_{\mathrm{y}} \\ \gamma_{\mathrm{xy}} \end{bmatrix} \\ \begin{bmatrix} \gamma_{\mathrm{yz}} \\ \gamma_{\mathrm{xz}} \end{bmatrix} \end{bmatrix}$$

$$= \begin{bmatrix} \boldsymbol{Q} & \boldsymbol{0}_{3\times 2} \\ \boldsymbol{0}_{2\times 3} & \boldsymbol{Q}_{\mathrm{s}} \end{bmatrix} \begin{bmatrix} \begin{bmatrix} \varepsilon_{\mathrm{x}} \\ \varepsilon_{\mathrm{y}} \\ \gamma_{\mathrm{xy}} \end{bmatrix} \\ \begin{bmatrix} \gamma_{\mathrm{yz}} \\ \gamma_{\mathrm{xz}} \end{bmatrix} \end{bmatrix} \tag{5}$$

where E, v, and G denote the material properties of the metallic panel. Based on Reissner–Mindlin theory [15, 25], the constitutive equations for the isotropic metallic panel are:

$$\begin{cases} \boldsymbol{N} = \boldsymbol{A}\left(\boldsymbol{\varepsilon}_{\mathrm{m}} + \boldsymbol{\varepsilon}_{\mathrm{mb}}\right) + \boldsymbol{B}\boldsymbol{k} \\ \boldsymbol{M} = \boldsymbol{B}\left(\boldsymbol{\varepsilon}_{\mathrm{m}} + \boldsymbol{\varepsilon}_{\mathrm{mb}}\right) + \boldsymbol{D}\boldsymbol{k} \\ \boldsymbol{R} = \boldsymbol{A}_{\mathrm{s}}\boldsymbol{\gamma} \end{cases} \tag{6}$$

where

$$(\boldsymbol{A},\boldsymbol{B},\boldsymbol{D}) = \int_{-h/2}^{h/2} \left(1, z, z^2\right) \boldsymbol{Q}\mathrm{d}z \tag{7}$$

$$\boldsymbol{A}_{\mathrm{s}} = \int_{-h/2}^{h/2} \boldsymbol{Q}_{\mathrm{s}}\mathrm{d}z \tag{8}$$

where $\boldsymbol{N}$, $\boldsymbol{M}$, and $\boldsymbol{R}$ are the membrane force vector, the bending moment vector, and the transverse shear force vector, respectively. $\boldsymbol{A}$, $\boldsymbol{B}$, $\boldsymbol{D}$, and $\boldsymbol{A}_{\mathrm{s}}$ are the membrane stretching stiffness matrices, the bending–stretching coupling stiffness matrices, the bending stiffness matrices, and the shear stiffness matrices, respectively. The piston aerodynamic load is [12,15,25]

$$\begin{aligned} p_{\mathrm{a}} &= -\frac{2q_a}{\beta}\left(\frac{\partial w}{\partial x} + \frac{Ma^2-2}{Ma^2-1}\frac{1}{V_\infty}\frac{\partial w}{\partial t}\right) \\ &= -\left(\lambda\frac{D_{110}}{a^3}\frac{\partial w}{\partial x} + \sqrt{\lambda R_M}\frac{D_{110}}{\omega_0 a^4}\frac{\partial w}{\partial t}\right) \end{aligned} \tag{9}$$

or in the form of nodal force,

$$\begin{aligned} \boldsymbol{p}_{\mathrm{a}} = -\Bigg(&\lambda\frac{D_{110}}{a^3}\left(\frac{\partial \boldsymbol{H}_{\mathrm{w}}}{\partial x}\boldsymbol{w}_{\mathrm{b}} + \frac{\partial \boldsymbol{H}_{\mathrm{w}\varphi}}{\partial x}\boldsymbol{w}_{\varphi}\right) \\ &+ \sqrt{\lambda R_{\mathrm{M}}}\frac{D_{110}}{\omega_0 a^4}\left(\boldsymbol{H}_{\mathrm{w}}\dot{\boldsymbol{w}}_{\mathrm{b}} + \boldsymbol{H}_{\mathrm{w}\varphi}\dot{\boldsymbol{w}}_{\varphi}\right)\Bigg) \end{aligned} \tag{10}$$

where $q_{\mathrm{a}} = \frac{1}{2}\rho_{\mathrm{a}}V_\infty^2$ denotes the mean flow dynamic pressure, V_∞ denotes the mean flow velocity, ρ_{a} denotes the air density, Ma denotes Mach number, D_{110} denotes the first element $\boldsymbol{D}\begin{pmatrix}1, & 1\end{pmatrix}$ of the bending stiffness matrix $\boldsymbol{D}$ in Eq. (6), $\lambda = \frac{2q_a a^3}{\beta D_{110}}$ denotes the non-dimensional dynamical pressure with $\beta = \sqrt{Ma^2-1}$, and a is the panel length along the stream direction. The aerodynamic damping coefficient is $R_{\mathrm{M}} = \left(\frac{Ma^2-2}{Ma^2-1}\right)^2\frac{\mu}{\beta}$, with the air–panel mass ratio $\mu = \frac{\rho_{\mathrm{a}}a}{\rho h}$. For $Ma \gg 1$, $R_{\mathrm{M}} \approx \frac{\mu}{Ma}$, and $R_{\mathrm{M}} = 0.1$ is selected [12,15,26].

The exerted Gaussian-type random acoustic excitation is specified by its power spectrum density function as [12,13,15]:

$$S(f) = \begin{cases} P_{\mathrm{ref}}^2 \times 10^{\mathrm{SPL}/10}, & 0 \le f \le f_{\mathrm{c}} \\ 0, \quad \text{otherwise} \end{cases} \tag{11}$$

where $P_{\mathrm{ref}} = 20\,\mu\mathrm{Pa}$ is the reference pressure, f_{c} is the selected cutoff frequency in Hertz, and SPL is the sound

pressure level in decibels (dB). Using the principle of virtual work, the governing equation can be obtained as [12,15]:

$$\begin{bmatrix} \boldsymbol{M}_{\mathrm{B}} & \boldsymbol{0} \\ \boldsymbol{0} & \boldsymbol{M}_{\mathrm{m}} \end{bmatrix} \begin{bmatrix} \ddot{\boldsymbol{W}}_{\mathrm{B}} \\ \ddot{\boldsymbol{W}}_{\mathrm{m}} \end{bmatrix} + \begin{bmatrix} \boldsymbol{C}_{A} & \boldsymbol{0} \\ \boldsymbol{0} & \boldsymbol{0} \end{bmatrix} \begin{bmatrix} \dot{\boldsymbol{W}}_{\mathrm{B}} \\ \dot{\boldsymbol{W}}_{\mathrm{m}} \end{bmatrix} + \left(\begin{bmatrix} \boldsymbol{K}_{\mathrm{B}} & \boldsymbol{K}_{\mathrm{Bm}} \\ \boldsymbol{K}_{\mathrm{mB}} & \boldsymbol{K}_{\mathrm{m}} \end{bmatrix} + \begin{bmatrix} \boldsymbol{K}_{\mathrm{A}} & \boldsymbol{0} \\ \boldsymbol{0} & \boldsymbol{0} \end{bmatrix} + \tfrac{1}{2} \begin{bmatrix} \boldsymbol{K}1_{\mathrm{B}} & \boldsymbol{K}\boldsymbol{1}_{\mathrm{Bm}} \\ \boldsymbol{K}\boldsymbol{1}_{\mathrm{mB}} & \boldsymbol{0} \end{bmatrix} + \tfrac{1}{3} \begin{bmatrix} \boldsymbol{K}2_{\mathrm{B}} & \boldsymbol{0} \\ \boldsymbol{0} & \boldsymbol{0} \end{bmatrix} \right) \times \begin{bmatrix} \boldsymbol{W}_{\mathrm{B}} \\ \boldsymbol{W}_{\mathrm{m}} \end{bmatrix} = \begin{Bmatrix} \boldsymbol{p}_{\mathrm{B}} \\ \boldsymbol{0} \end{Bmatrix} \tag{12}$$

where $\boldsymbol{M}_{\mathrm{B}}$ and $\boldsymbol{M}_{\mathrm{m}}$ denote the system mass matrices affected by the bending–stretching, membrane displacements, respectively. $\boldsymbol{C}_{\mathrm{A}}$denotes the aerodynamic damping matrix. $\boldsymbol{K}$, $\boldsymbol{K}1$, and $\boldsymbol{K}2$ denote the linear, first-order and second-order nonlinear stiffness matrices. The nonlinear stiffness terms depend linearly and quadratically on displacements, the subscript B, and m denote the bending–stretching, membrane-related components, respectively. $\boldsymbol{p}_{\mathrm{B}}$ is the nodal random forces. By neglecting the membrane inertia term, the membrane displacement vector can be expressed as [12,15]:

$$\boldsymbol{W}_{\mathrm{m}} = -\boldsymbol{K}_{\mathrm{m}}^{-1}\boldsymbol{K}_{\mathrm{mB}}\boldsymbol{W}_{\mathrm{B}} - \frac{1}{2}\boldsymbol{K}_{\mathrm{m}}^{-1}\boldsymbol{K}1_{\mathrm{mB}}\boldsymbol{W}_{\mathrm{B}} \tag{13}$$

Then, the governing equation can be written in terms of the bending displacement,

$$\boldsymbol{M}_{\mathrm{B}}\ \ddot{\boldsymbol{W}}_{\mathrm{B}} + \boldsymbol{C}_{\mathrm{A}}\dot{\boldsymbol{W}}_{\mathrm{B}} + \left(\begin{matrix} \boldsymbol{K}_{\mathrm{B}} - \boldsymbol{K}_{\mathrm{T}} + \boldsymbol{K}_{\mathrm{A}} \\ +\frac{1}{2}\boldsymbol{K}1_{\mathrm{B}} + \frac{1}{3}\boldsymbol{K}2_{\mathrm{B}} \end{matrix} \right) \boldsymbol{W}_{\mathrm{B}} + \left(\boldsymbol{K}_{\mathrm{Bm}} + \frac{1}{2}\boldsymbol{K}1_{\mathrm{Bm}} \right) \underbrace{\begin{pmatrix} -\boldsymbol{K}_{\mathrm{m}}^{-\boldsymbol{1}}\boldsymbol{K}_{\mathrm{mB}}\overline{\boldsymbol{w}_{\mathrm{B}}} \\ -\frac{1}{2}\boldsymbol{K}_{\mathrm{m}}^{-1}\boldsymbol{K}\boldsymbol{1}_{\mathrm{mB}}\overline{\boldsymbol{w}_{\mathrm{B}}} \end{pmatrix}}_{\boldsymbol{W}_{\mathrm{m}}} = \boldsymbol{p}_{\mathrm{B}} \tag{14}$$

As the bending displacement $\boldsymbol{W}_{\mathrm{B}}$can be expressed as a linear combination of normal transverse modes as:

$$\boldsymbol{W}_{\mathrm{B}} = \boldsymbol{Q}\boldsymbol{q}\,(t) \approx \sum_{r=1}^{N} \boldsymbol{Q}_r q_r\,(t) \tag{15}$$

where $\boldsymbol{Q} = \left[\boldsymbol{Q}_1\ \boldsymbol{Q}_2 \cdots \boldsymbol{Q}_{\mathrm{N}}\right]$ is the selected natural mode shapes of the panel obtained from a derived eigenproblem without the thermal effect of Eq. (12) as:

$$\omega_r^2 \boldsymbol{M}_{\mathrm{B}}\boldsymbol{Q}_r = \left(\boldsymbol{K}_{\mathrm{B}} - \boldsymbol{K}_{\mathrm{Bm}}\boldsymbol{K}_{\mathrm{m}}^{-1}\boldsymbol{K}_{\mathrm{mB}}\right)\boldsymbol{Q}_r \tag{16}$$

Accordingly, the system governing equations in Eq. (12) can be transformed into the modal coordinates as:

$$\overline{\boldsymbol{M}_{\mathrm{B}}}\ddot{\boldsymbol{q}} + \overline{\boldsymbol{C}_{\mathrm{A}}}\dot{\boldsymbol{q}} + 2\xi_r f_r \boldsymbol{I}\overline{\boldsymbol{M}_{\mathrm{B}}}\dot{\boldsymbol{q}} + \left(\overline{\boldsymbol{K}_{\mathrm{L}}} + \overline{\boldsymbol{K}_{\mathrm{NL}}}\right)\boldsymbol{q} = \overline{\boldsymbol{P}_{\mathrm{B}}} \tag{17}$$

where the terms with superscript denote the corresponding matrices in the modal system, and,

$$\left(\overline{\boldsymbol{M}_{\mathrm{B}}}, \overline{\boldsymbol{C}_{\mathrm{A}}}, \overline{\boldsymbol{K}_{\mathrm{L}}}\right) = \boldsymbol{Q}^{\mathrm{T}}\left(\boldsymbol{M}_{\mathrm{B}}, \boldsymbol{C}_{\mathrm{A}}, \left(\boldsymbol{K}_{\mathrm{B}} + \boldsymbol{K}_{\mathrm{A}} - \boldsymbol{K}_{\mathrm{Bm}}\boldsymbol{K}_{\mathrm{m}}^{-1}\boldsymbol{K}_{\mathrm{mB}}\right)\right)\boldsymbol{Q} \tag{18}$$

$$\overline{\boldsymbol{K}_{\mathrm{NL}}} = \boldsymbol{Q}^{\mathrm{T}}\left(\frac{1}{2}\boldsymbol{K}\boldsymbol{1}_{\mathrm{B}} + \frac{1}{3}\boldsymbol{K}\boldsymbol{2}_{\mathrm{B}} - \frac{1}{2}\boldsymbol{K}_{\mathrm{Bm}}\boldsymbol{K}_{\mathrm{m}}^{-1}\boldsymbol{K}1_{\mathrm{mB}} - \frac{1}{2}\boldsymbol{K}1_{\mathrm{Bm}}\boldsymbol{K}_{\mathrm{m}}^{-1}\boldsymbol{K}_{\mathrm{mB}} - \frac{1}{4}\boldsymbol{K}\boldsymbol{1}_{\mathrm{Bm}}\boldsymbol{K}_{\mathrm{m}}^{-1}\boldsymbol{K}1_{\mathrm{mB}}\right)\boldsymbol{Q} \tag{19}$$

$$\overline{\boldsymbol{P}_{\mathrm{B}}} = \boldsymbol{Q}^{\mathrm{T}}\boldsymbol{p}_{\mathrm{B}} \tag{20}$$

Considering the structural damping effect, a structural modal damping matrix $2\xi_r f_r \boldsymbol{I}\overline{\boldsymbol{M}_{\mathrm{B}}}$has been added to Eq. (17). The coefficient $\xi_r = 0.01$ is the modal damping ratio of the rth mode, and f_r is the corresponding natural frequency. Finally, the fourth-order Runge–Kutta integration method is employed to obtain the dynamic response. Equation (17) can be rewritten in the state space, and the fourth-order Runge–Kutta numerical integration method with a fixed time step of 1/5000 s is adopted to solve the dynamic differential equations, while a random acoustic loading is generated with the same time step [12,13,15].

3 Numerical results and discussions

The properties of a fully clamped square metallic panel are listed in Table 1.

For panel subjected to combined aerodynamic and acoustic load, the location of the maximum deflection is not at a fixed position, the position could be somewhere between the panel center and the three quarter from the leading edge, and the reference point is fixed at (3a/4, a/2) in this study [12,15].

Table 1 Geometric and material properties of a fully clamped square panel

Geometric properties	Material properties (Ti-6242S)
Dimensions a × a × h: 0.3 m × 0.3 m × 0.001 m	$E = 113\,\text{GPa}$
Boundary conditions: clamped (C–C–C–C)	$G = 46\,\text{GPa}$
Poisson's ratio: ν=0.3	Density: $\rho = 4370\ \text{Kg}\,\text{m}^{-3}$

Table 2 Natural frequencies (Hz) of the fully clamped square titanium plate

Mode order	1	2	3	4	5	6	7	8
Type	Symmetric	Anti-symmetric	Anti-symmetric	Symmetric	Anti-symmetric	Anti-symmetric	Antisymmetric	Anti-symmetric
NASTRAN	97.96	199.80	199.90	294.84	358.40	360.09	449.49	449.97
FEM (MIN3)	98.67	201.76	201.99	299.22	366.25	367.88	458.16	460.67
Err., %	0.73	0.98	1.04	1.49	2.19	2.16	1.92	2.38

Table 3 Modal convergence study

Selected modes number	RMS (W/h)
6	0.4928
12	0.7838
16	0.7843
26	0.7848
30	0.7848

3.1 Validation of the formulation

Firstly, the proposed finite element method is verified in this section. The system natural frequencies obtained by Eq. (16) are compared with those obtained by MSC/NASTRAN as listed in Table 2. It can be seen that they are in good agreement. Thus, the triangular meshes (20 × 20 × 2) with MIN3 element can be employed to model the metallic panel for further dynamic analysis [15].

Then, the convergence study for building reduced-order model under combined loads (SPL = 120 dB, $\lambda = 1000$) is conducted as listed in Table 3, the obtained results are listed in Table 3, and it can be clearly shown that the first twenty-six modes can be employed for the following numerical cases analysis with enough accuracy.

Finally, the limit-cycle oscillation amplitudes obtained by using the proposed method agree well with the open literature [26,27] as shown in Fig. 2; thus, the capability of the proposed finite element method to calculate the flutter motion is validated [15].

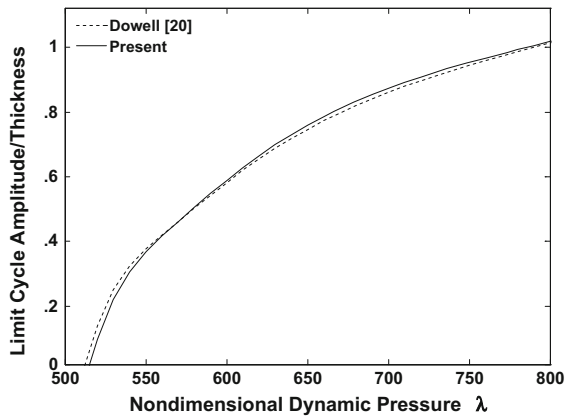

Fig. 2 Comparison of limit-cycle oscillation amplitudes [15]

3.2 Aeroelastic effect on the overall response

After the proposed finite element method is verified, considering that the aerodynamic load can function as aerodynamic stiffness and damping within the updated aeroelastic model as described in Eq. (14), it is also necessary to calculate the variation of the natural frequencies of the aeroelastic model as shown in Fig. 3. It can be clearly shown that the first three natural frequencies can be remarkably regulated by the increasing flow dynamic pressure λ. And the frequencies merging procedure between the first two aeroelastic modes can be observed as the flow dynamic pressure increases. These two frequencies merge at the critical aerodynamic pressure, $\lambda_{cr} = 812$.

Based on the obtained panel natural frequencies with null aerodynamic load listed in Table 2, from the per-

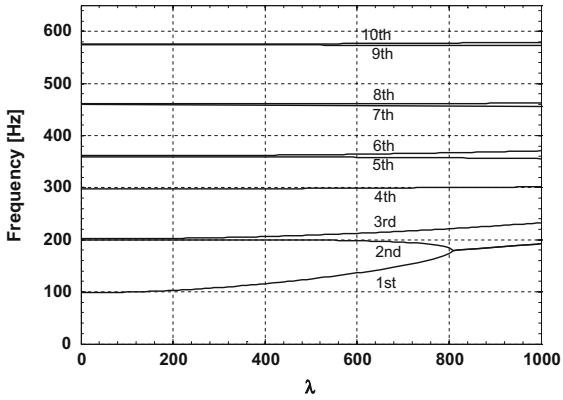

Fig. 3 Variation of natural frequencies with increasing flow dynamic pressure

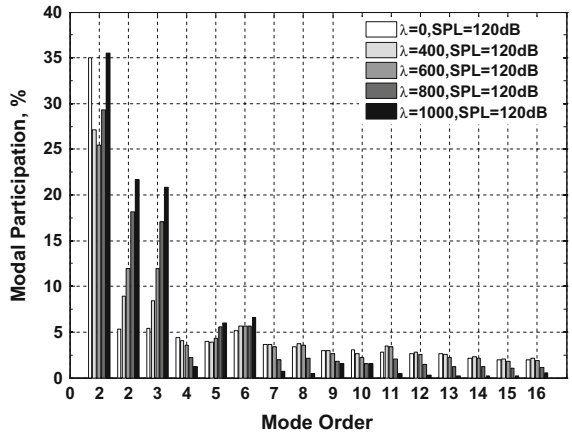

Fig. 4 Variation of modal participation distribution

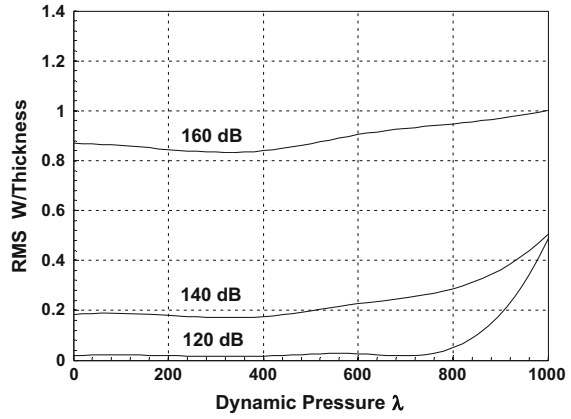

Fig. 5 RMS response versus flow dynamic pressure λ with different SPL

spective of the internal/external resonances, there exist some nearly integral ratios: one-to-one 1:1 relationships among these natural frequencies (such as mode 2nd and 3rd, mode 5th and 6th, mode 7th and 8th, respectively), one-to-two 1:2 (for mode 1st and 2nd. In fact, for this specific square panel, each antisymmetric mode has a companion mode. Therefore, internal resonances of the type one-to-one (1:1) can be always presented with different modal participation [17,18,20]. Thus in this case, the modal internal resonances are largely affected by the variation of the natural frequencies as the flow dynamic pressure changes; thus, the modal interaction mechanism can be altered [17,20]. To quantify the aeroelastic effect on the modal interaction mechanism, the variation of modal participation of panel random vibrations under SPL = 120 dB with different flow dynamic pressures is presented in Fig. 4. The modal participation value is defined as Eq. (21), where RMS denotes root-mean-square of the random deflections [28].

$$\text{Participation of the } r\text{th mode} = \frac{\text{RMS}\,|q_r|}{\sum_{s=1}^{N}\text{RMS}\,|q_s|} \tag{21}$$

From Fig. 4, it can be seen that as the flow dynamic pressure increases from zero to 1000, the modal participation of the lower twin modes (2nd and 3rd, 5th and 6th) increases with the almost same participation level, but the modal participation of the higher modes decreases. These changes indicate that more energy be transferred from the higher modes to the lower modes as the flow dynamics pressure increases. Within the lower modes (mode 1st–6th), as the flow dynamic pressure increases, the modal participation of the mode 1st initially decreases and then increases, and the 4th mode participation continues to decrease.

As each mode modal participation can be significantly regulated by the increasing flow dynamic pressure, thus the dynamic behavior can be consequently altered. Figure 5 illustrates the overall RMS response of deflections under varying combined loads. Before the flutter occurrence, the deflections decrease as the flow dynamic pressure increases. Thus, the system is stiffened by the additive aerodynamic load due to aeroelastic effect. As the dynamic pressure is approaching the critical flutter value $\lambda_{cr} = 812$, there exist smooth transitions prior to the flutter limit-cycle oscillations (LCOs). And in the post-flutter region, the deflections

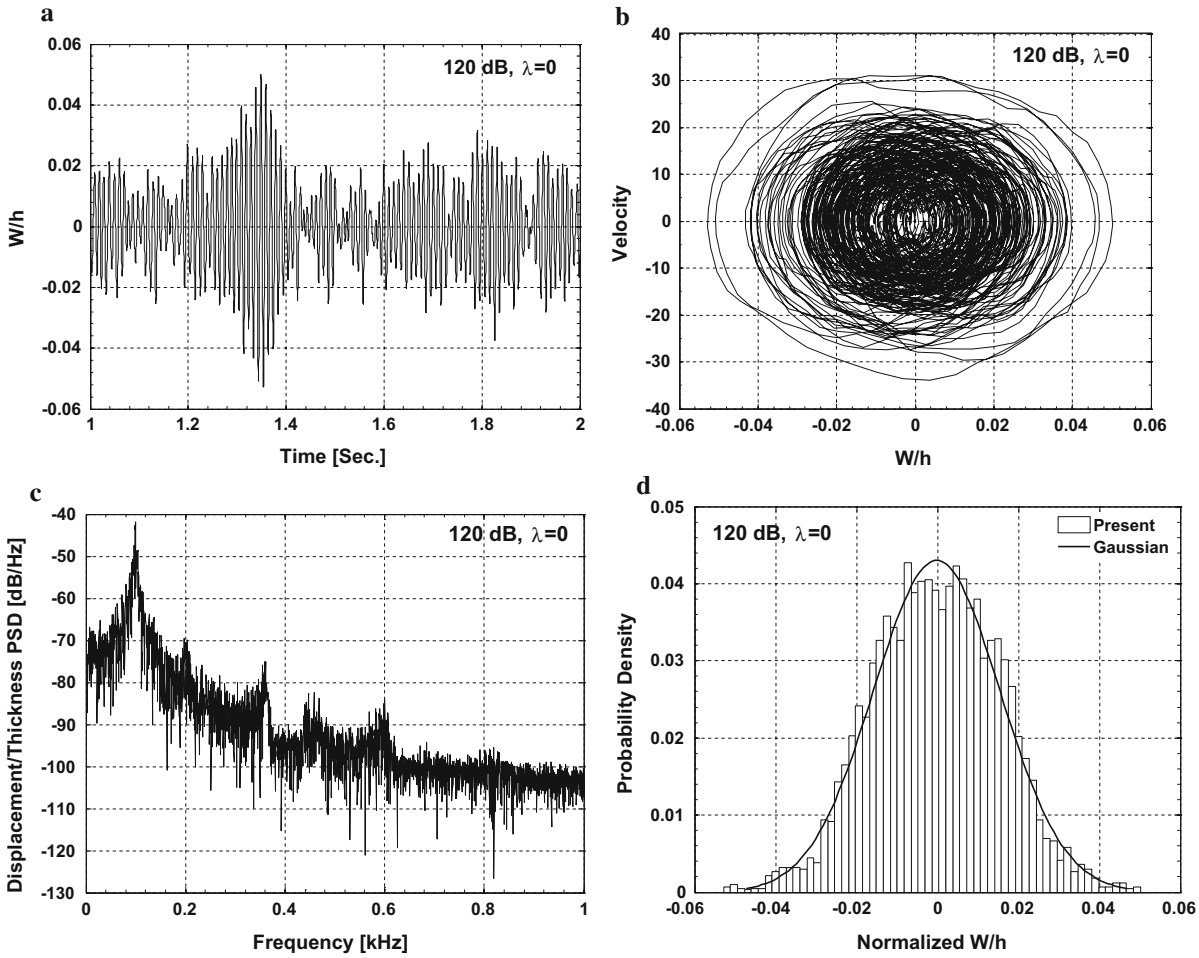

Fig. 6 Random response (SPL = 120 dB, λ = 0, RMS = 0.0182). **a** Non-dimensional deflection time history. **b** Phase plane.**c** Displacement spectral density. **d** Probability density distribution for displacement

can always be higher than those without aerodynamic load as the flow dynamic pressure increases to the high enough level [12]. These characteristics coincide with the variation of modal participation of the fundamental mode as shown in Fig. 4. To obtain more detailed knowledge of these complex behaviors, some representative cases under different combination loads are presented in the flowing sections.

3.3 Cases studies

3.3.1 Random vibration response without aeroelastic effect

In this section, two cases with null aerodynamic load are presented firstly to give us some basic knowledge of pure random vibration response. Figures 6 and 7 illustrate the random vibrations with null aerodynamic pressure (λ = 0) at sound pressure levels SPL = 120 and 160 dB, respectively. At sound pressure level SPL = 120 dB, the panel basically experiences a small deflection linear random vibration. The deflections power spectrum density (PSD) responses are shown in Fig. 6c. According to the calculated natural frequencies and modal participation distribution (Table 2; Figs. 3, 4), the deflections PSD of the linear random response (SPL = 120 dB, λ = 0) is dominated by the fundamental resonant peak [1st symmetric mode (1,1)] in the fashion of external resonance, which is excited by the spatially uniform, random acoustic load. Even that the second natural frequency is twice the first one, however, this nearly integer ratio of natural

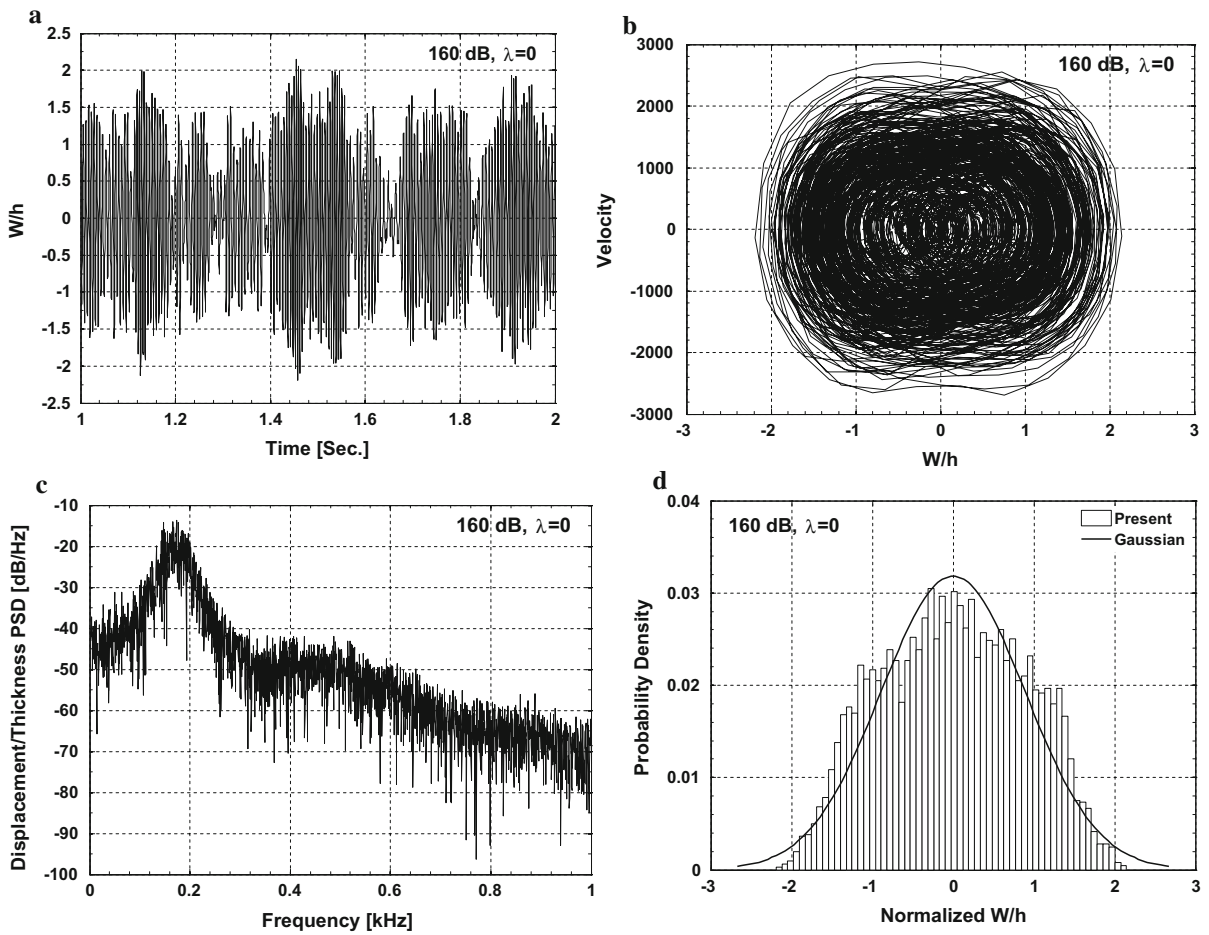

Fig. 7 Random response (SPL = 160 dB, λ = 0, RMS = 0.8691). **a** Non-dimensional deflection time history, **b** phase plane. **c** Displacement spectral density. **d** Probability density distribution for displacement

frequencies does not guarantee a significant one-to-two (1:2) internal resonances (Figs. 4, 6).

While at SPL = 160 dB, λ = 0, the panel experiences a larger deflection nonlinear random vibration as shown in Fig. 7. The deflections PSD responses are shown in Fig. 7c. In this nonlinear vibration case, the fundamental resonance peak becomes flattened and shifts to the higher-frequency region (around 160 Hz) due to the hardening-type nonlinear frequency–amplitude relationship induced by the large deflections. This relationship figures out that for a nonlinear dynamic system with positive linear and nonlinear stiffness, there exist some unstable multi-valued frequency regions in the higher-frequency region relative to the linear resonance peaks [15,23]. Based on the PSD analysis of these two cases, both of which are dominated by one single resonance peak, it is reasonable that the single-degree-of-freedom(SDOF) model be always adopted in the previous thermo-acoustic studies [2,11]. As different PSD responses can be accompanied with different deflections probability density distributions, in the linear case (Fig. 6d), the deflections probability density distribution is close to Gaussian, while in the nonlinear case (Fig. 7d), the initial Gaussian-type distribution can be flattened caused by the multi-valued hardening- type frequency–amplitude relationship due to large deflections. Thus, the phenomenon bifurcation (P-bifurcation) due to the intensified random excitation can be observed [23].

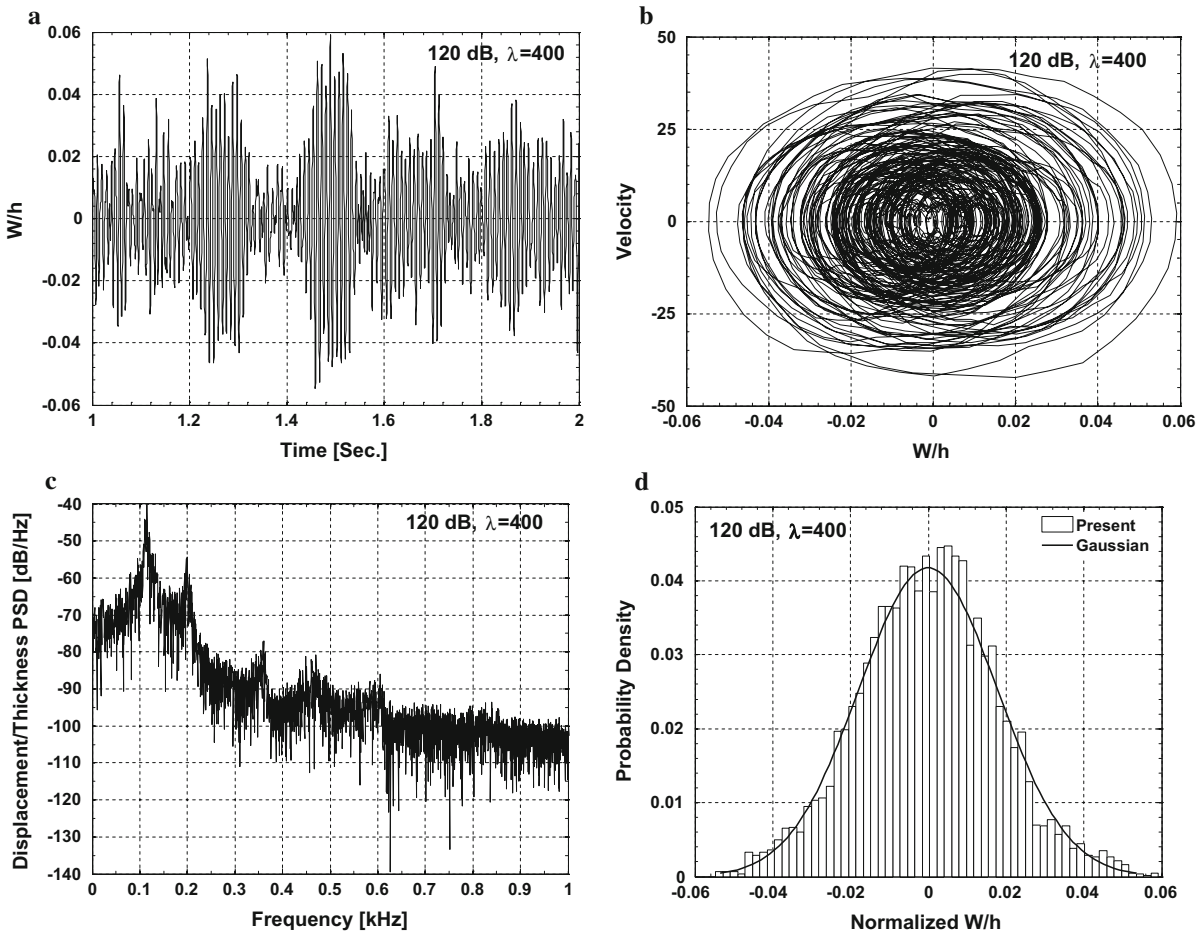

Fig. 8 Random response (SPL = 120 dB, $\lambda = 400$, RMS = 0.0180). **a** Non-dimensional deflection time history. **b** Phase plane. **c** Displacement spectral density. **d** Probability density distribution for displacement

3.3.2 Aeroelastic effect on random vibration in the pre-/near-flutter regions

Before studying the aeroelastic effect on the panel random vibration, the critical flutter aerodynamic pressure $\lambda_{cr} = 812$ is calculated to classify different regions as pre-flutter region ($\lambda \ll \lambda_{cr}$), near-flutter region ($\lambda < \lambda_{cr}$), and post-flutter region ($\lambda > \lambda_{cr}$). As the proposed model does not consider the perturbations on the mean flow velocity due to boundary layer [3,4,15], thus the aeroelastic system stability can be independent with the exerted random acoustic excitation. Based on the variation of natural frequencies with changing dynamic pressure (Fig. 3), it is clearly shown that in the pre-flutter region, when the flow dynamic pressure λ is increased to 400, the fundamental mode natural frequency increases lightly, while its modal participation decreases (Fig. 4), thus the panel experiences a linear random vibration with lower amplitudes as shown in Fig. 8. These changes can be illustrated as a shifted fundamental resonant peak in the deflections PSD response, which is different with its counterpart of the linear case (SPL = 120 dB, $\lambda = 0$).

Under SPL = 120 dB and $\lambda = 800$, in the near-flutter region, the panel also experiences a linear random vibration as shown in Fig. 9 with increased amplitudes. It can be seen in Fig. 4 that much more participation are contributed by the lower three modes in this case. In the PSD response as shown in Fig. 9c, the almost merged frequencies of the first two aeroelastic modes can be observed. And these changes in the PSD response demonstrate that it is necessary to consider

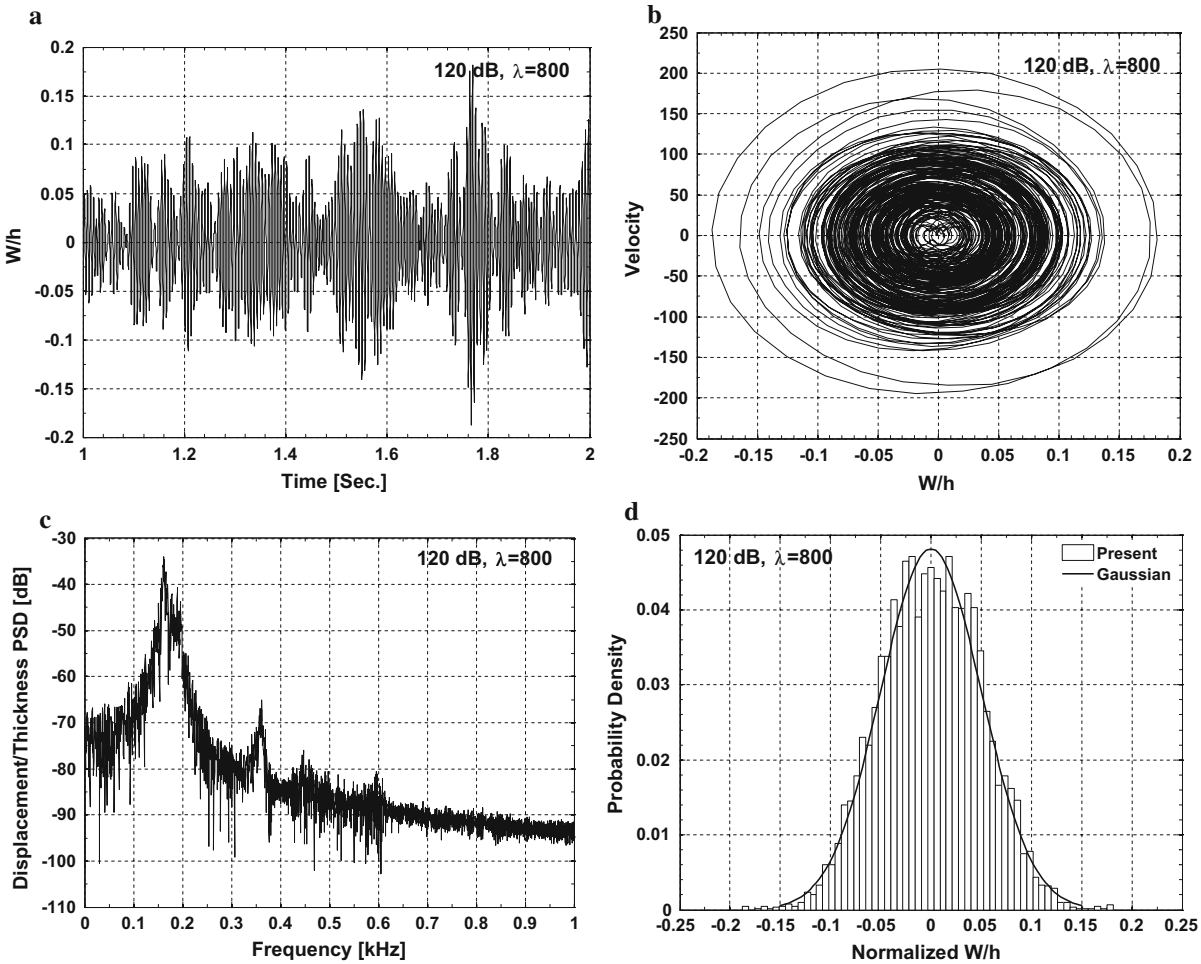

Fig. 9 Random response (SPL = 120 dB, λ = 800, RMS = 0.0806). **a** Non-dimensional deflection time history. **b** Phase plane. **c** Displacement spectral density. **d** Probability density distribution for displacement

the aeroelastic effect for a more accurate response prediction even before the flutter occurrence. Additionally, the deflections probability density distributions of these two cases are both close to Gaussian.

The above cases all illustrate the linear random vibration under random acoustic excitation with lower SPL. The following two cases will discuss the random vibration under higher-level random excitation, SPL = 160 dB. The case (SPL = 160 dB, λ = 0) is illustrated in Fig. 7, and the variation of modal participation with increasing flow dynamic pressures under SPL = 160 dB is presented in Fig. 10. It can be clearly shown that the modal participation of the fundamental mode decreases, while higher-order modal participation increases as the flow dynamic pressure

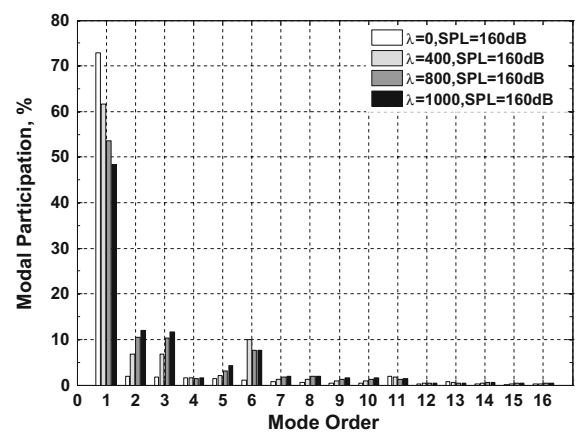

Fig. 10 Variation of modal participation distribution under SPL = 160 dB

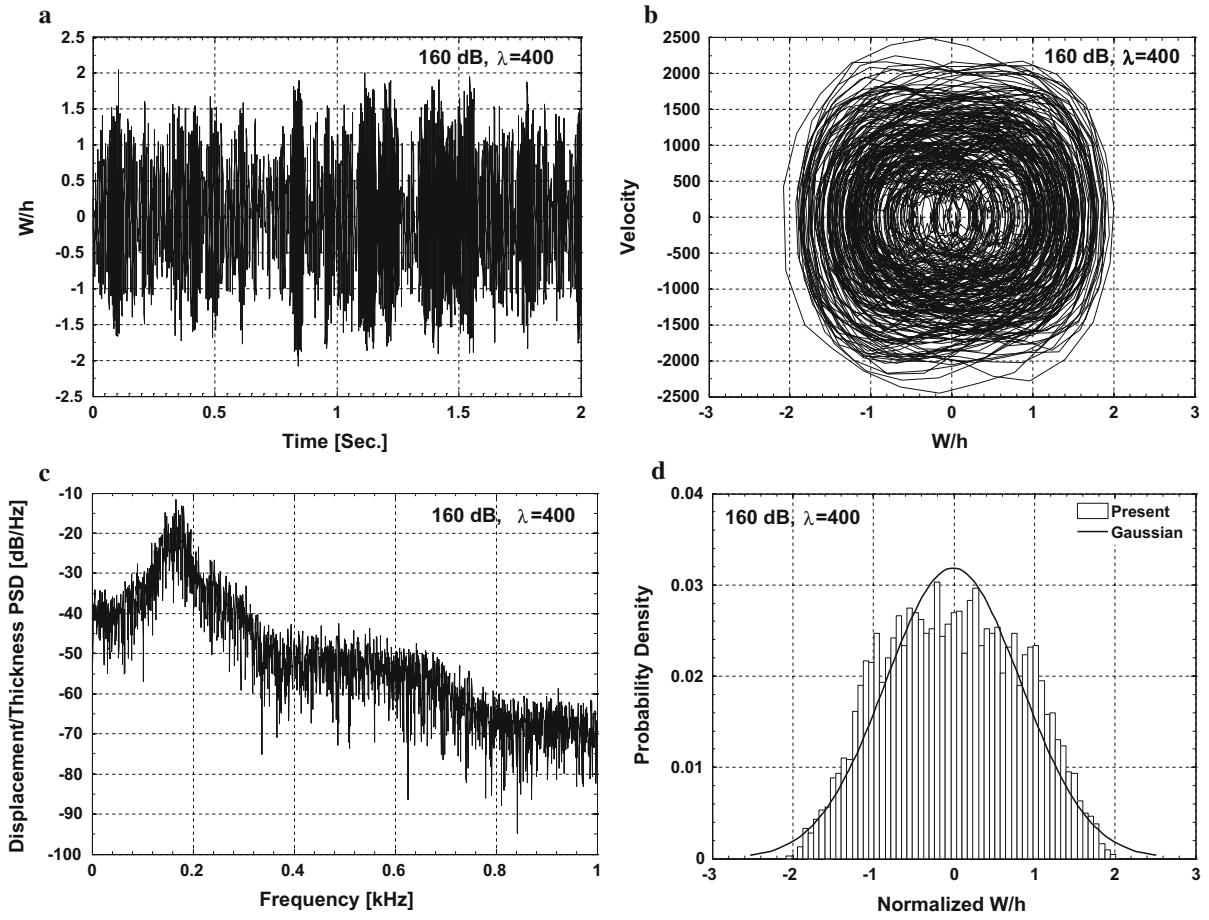

Fig. 11 Random response (SPL = 160 dB, λ = 400, RMS = 0.8395). **a** Non-dimensional deflection time history. **b** Phase plane. **c** Displacement spectral density. **d** Probability density distribution for displacement

λ increases. Comparing with the modal participation variation under SPL = 120 dB shown in Fig. 4, the first mode modal participation in this case can be much higher than its counterpart to dominate the overall dynamic behavior.

At (SPL = 160 dB, λ = 400), the panel mainly experiences a large deflection nonlinear random vibration as shown in Fig. 11. Comparing with the nonlinear case with null flow dynamic pressure shown in Fig. 7, the deflections of this case decrease due to the additive aerodynamic stiffness. As the flow dynamic pressure increases to λ = 800 as shown in Fig. 12, the deflections increase, and there appear some higher resonant peaks in addition to the fundamental resonant peak as the probability density distributions of the non-dimensional deflections of these two cases (λ = 400, 800) both represent as the flatten distribution plateau.

3.3.3 Aeroelastic effect on random vibration in post-flutter region

As the exerted random acoustic excitation does not alter the system dynamic stability (panel flutter), a pure panel flutter case (λ=1000, SPL = 0 dB) is presented here to build a benchmark case for comparison as shown in Fig. 13. It can be shown in the phase plot that the panel mainly experiences typical LCOs. The flutter mechanism, coalescence of the first two aeroelastic coupled frequencies (Fig. 3), can be illustrated as a sharp merged resonant peak (≈ 189.5 Hz) as shown in Fig. 13c.

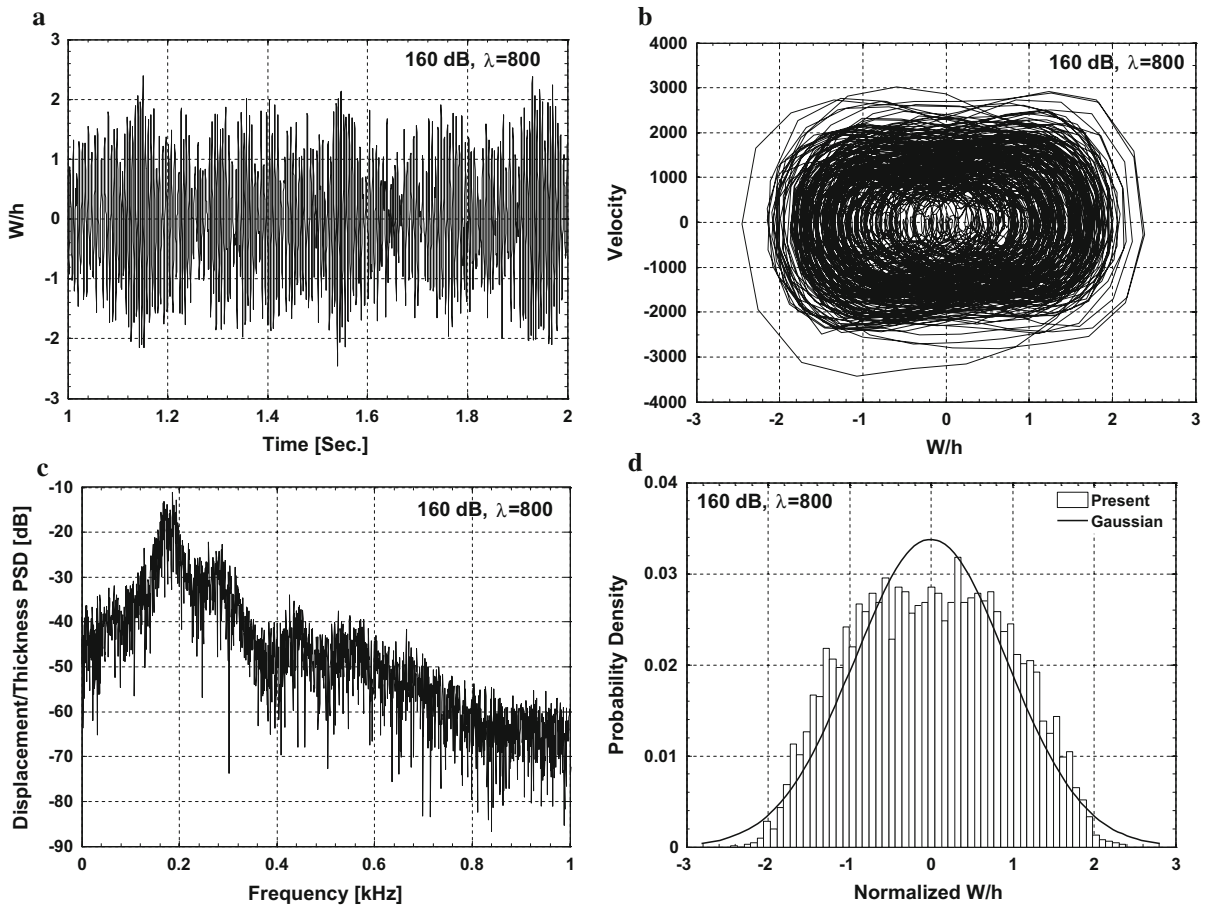

Fig. 12 Random response (SPL = 160 dB, λ = 800, RMS = 0.9370). **a** Non-dimensional deflection time history. **b** Phase plane. **c** Displacement spectral density. **d** Probability density distribution for displacement

In addition to the first two modes with 1:1 internal resonances [18], it can be seen in Fig. 14 that the modal contribution of the third mode keeps the almost same level with the second one. However, the PSD response is dominated by three sharp peaks with nearly integral ratio, 1:3:5, which indicates that the single periodic motion be enriched by its odd order superharmonic motions. With such a highly ordered spectrum response, it is reasonably assumed that the fluttering panel can function as a linear filter to the wideband excitation [29].

At SPL = 120 dB and λ=1000, based on the modal participation distribution (Fig. 14) of the vibrations under different combined loads in the post-flutter region, both the above two cases possess the almost same modal participation; thus, this case (SPL = 120 dB, λ = 1000) is dominated by the flutter motion. The corresponding behavior is shown in Fig. 15 as diffused limit-cycle oscillations. And the PSD response overall presents the characteristics of odd order superharmonic motions, while there exists a resonant peak indicating the third aeroelastic mode (Fig. 3) [30,31]. Comparing with the cases with single peak distributions in the pre-/near-flutter regions, the probability density distribution of non-dimensional deflections presents a fork-like shape with two peaks, indicating LCOs amplitudes as shown in Fig. 15d. This dynamic bifurcation [23], induced by the instability of this aeroelastic coupling system, can cause significant change of the mean and vibratory strains of the vibrating panel.

However, as the sound pressure level is increased to SPL = 160 dB, the characteristic of the modal participation distribution can be significantly altered as shown in Fig. 14. Figure 16 clearly shows that the initial odd

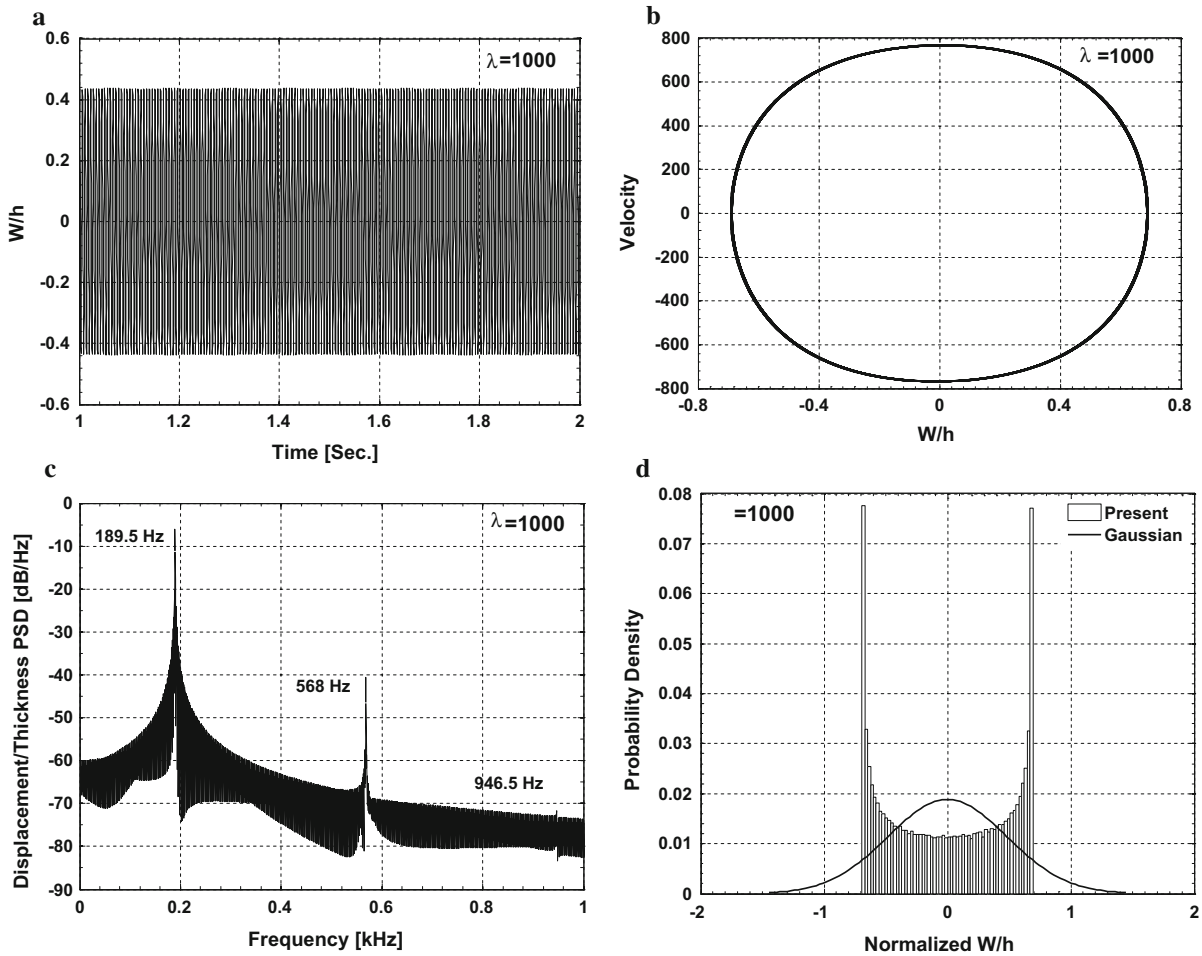

Fig. 13 Random response (SPL = 0 dB, λ = 1000, LCOs amplitudes, 0.4816). **a** Non-dimensional deflection time history, **b** phase plane, **c** displacement spectral density, **d** probability density distribution for displacement

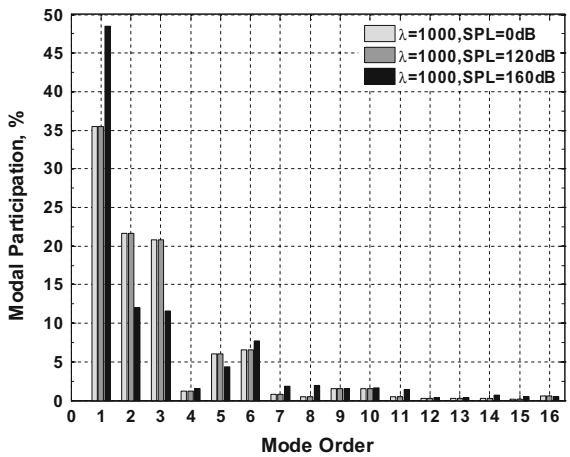

Fig. 14 Modal participation distribution in post-flutter region

order super-harmonic motion characterized by flutter motion can be replaced by external resonances; thus, the panel experiences a large deflection nonlinear random motion. And the PSD response (Fig. 16c) is dominated by a broaden fundamental resonant peak. Correspondingly, the deflections probability density distribution experiences another P-bifurcation shown as a plateau distribution in Fig. 16d.

4 Conclusions

Based on the first-order shear deformation plate theory and piston aerodynamic theory, the aeroelastic effect on both the modal interaction mechanism and dynamic behavior of acoustically excited panels is studied. As

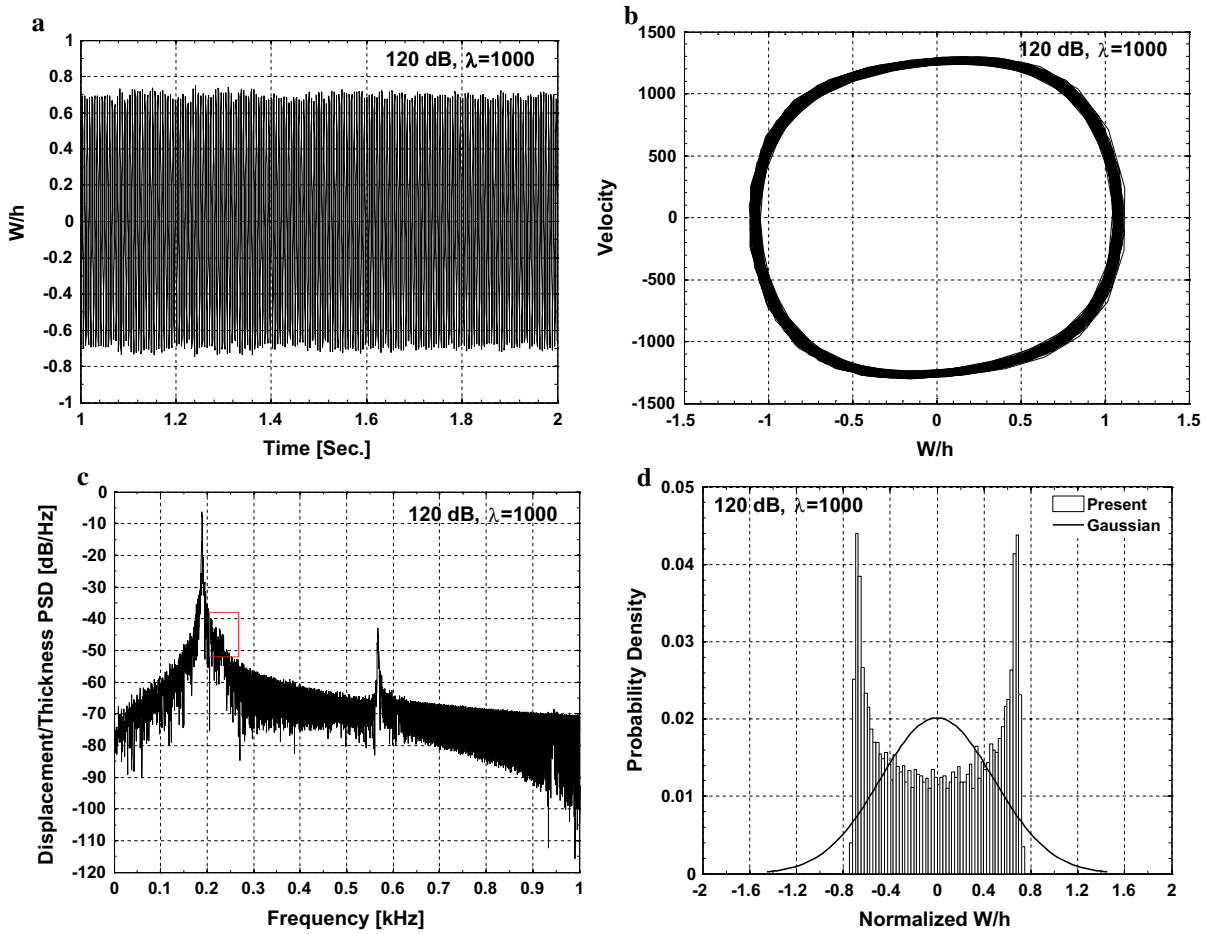

Fig. 15 Random response (SPL = 120 dB, λ = 1000). **a** Non-dimensional deflection time history. **b** Phase plane. **c** Displacement spectral density. **d** Probability density distribution for displacement

an extension work of studies [12,15], this paper emphasizes on analyzing the aeroelastic modal interaction mechanism; thus, the corresponding complex dynamic behavior can be better understood, and the following conclusions can be drawn.

1. Based on the variation of natural frequencies and modal participation with increasing flow dynamic pressure within the updated aeroelastic model, the aeroelastic modal interaction mechanism can be not only affected by the coupling mechanism between the first two approaching aeroelastic modes, which can lead to 1:1 internal resonance thus panel flutter, but also affected by the initial companion modes (especially the first twin companion modes). Additionally, the higher the flow dynamic pressure, the more participation contributed by the lower aeroelastic modes.
2. In the pre-/near-flutter regions, in addition to the dominant fundamental mode excited by the random acoustic excitation, the first twin companion antisymmetric modes (especially the second and third modes) can pose much more modal participation with the almost same level with the increasing flow dynamic pressure, while the modal participation of the dominant fundamental mode varies. These changing trends may explain the changing overall amplitudes RMS response with increasing flow dynamic pressure. Thus in this region, the panel behavior exhibits linear random vibrations.
3. In the post-flutter region, as the flutter LCOs are characterized by 1:1 internal resonances accom-

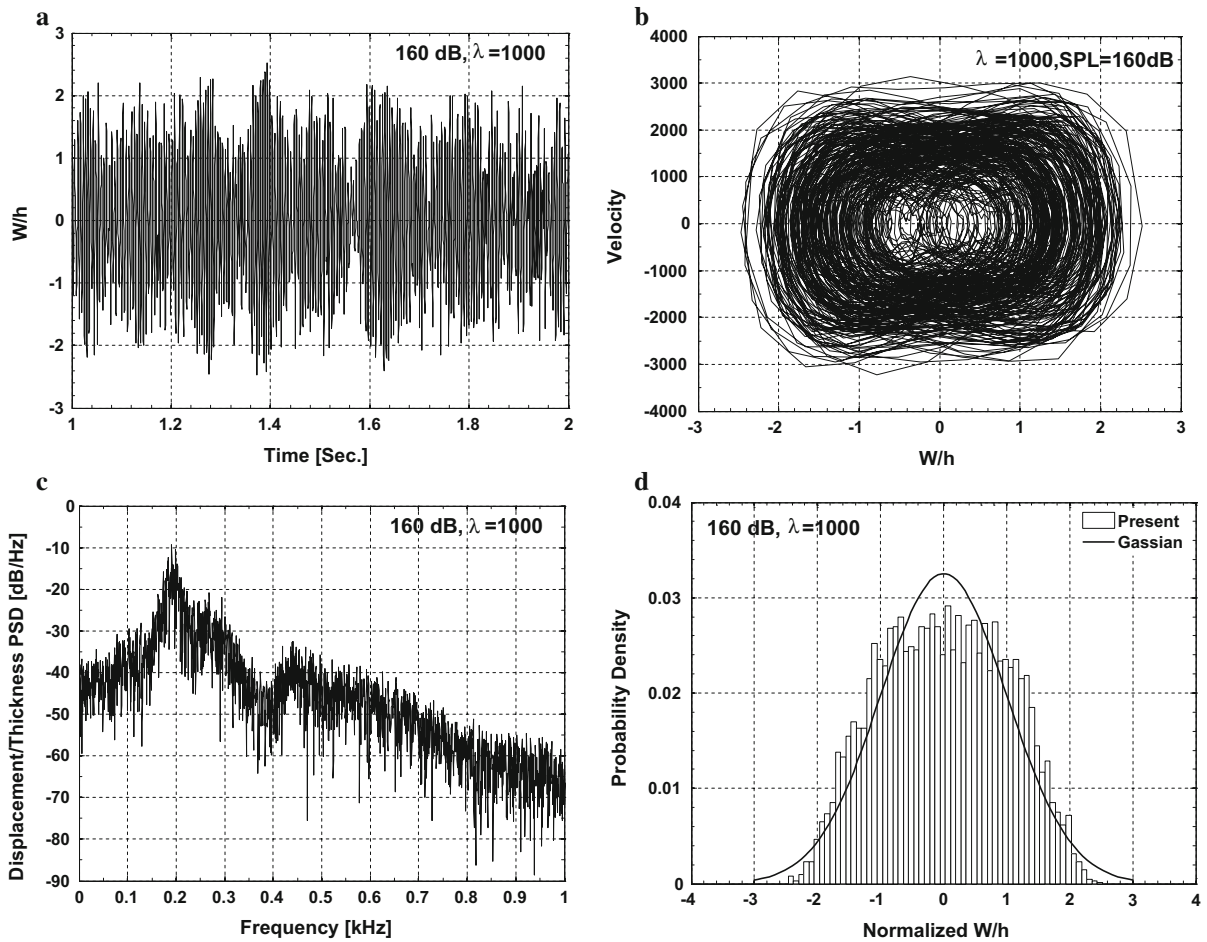

Fig. 16 Random response (SPL = 160 dB, λ = 1000). **a** Non-dimensional deflection time history. **b** Phase plane. **c** Displacement spectral density. **d** Probability density distribution for displacement

panied with its odd order super-harmonic motion; thus, the random motion can be highly ordered regulated. However, as much more modal participation of the fundamental mode can be caused by the intensifying random acoustic excitation, the specific aeroelastic modal participation distribution of flutter motion can be eliminated. Thus, the highly ordered LCO motion can be transformed into random motion.

4. Within this aeroelastic modal interaction mechanism, the vibration response can be also altered by the geometric nonlinearity due to large deflections through the nonlinear frequency–amplitude relationship. Correspondingly, various stochastic bifurcations can be observed.

Acknowledgements The presented work is supported by the National Natural Science Foundation of China (NSFC, Grant No. 11472216). The first author gratefully acknowledges the support from China Scholarship Council (CSC) and German Aerospace Center (DLR). The authors thank for helpful discussion of Dr. Wei Hu, Dr. Ning Guo, and Dr. Shun He.

References

1. Eason, T.G., Spottswood, S.M.: A structures perspective on the challenges associated with analyzing a reusable hypersonic platform. In: 54th AIAA/ASME/ASCE/AHS/ASC structures, structural dynamics, and materials conference. American Institute of Aeronautics and Astronautics (2013)
2. Pozefsky, P., Blevins, R.D, Laganelli, A.: Thermo-vibroacoustic loads and fatigue of hypersonic flight vehicle structure. AFRL TR 3014 (1989)

3. Miller, B.A., McNamara, J.J., Spottswood, S.M.: The impact of flow induced loads on snap-through behavior of acoustically excited, thermally buckled panels. J. Sound Vib. **330**(23), 5736–5752 (2011). doi:10.1016/j.jsv.2011.06.028
4. Fung, Y.C.: Some recent contributions to panel flutter research. AIAA J. **1**(4), 898–909 (1963). doi:10.2514/3.1661
5. Muhlstein, L., Gaspers, P.A., Riddle, D.W.: An experimental study of the influence of the turbulent boundary layer on panel flutter. National Aeronautics and Space Administration (1968)
6. Dowell, E.H.: Generalized aerodynamic forces on a flexible plate undergoing transient motion in a shear flow with an application to panel flutter. AIAA J. **9**(5), 834–841 (1971). doi:10.2514/3.6283
7. Vedeneev, V.: Interaction of panel flutter with inviscid boundary layer instability in supersonic flow. J. Fluid Mech. **736**, 216–249 (2013). doi:10.1017/jfm.2013.522
8. Hashimoto, A., Aoyama, T., Nakamura, Y.: Effects of turbulent boundary layer on panel flutter. AIAA J. **47**(12), 2785–2791 (2009). doi:10.2514/1.35786
9. Alder, M.: Development and validation of a partitioned fluid-Structure solver for transonic panel flutter with focus on boundary layer effects. In: 44th AIAA fluid dynamics conference. American Institute of Aeronautics and Astronautics (2014)
10. Ostoich, C.M., Bodony, D.J., Geubelle, P.H.: Interaction of a Mach 2.25 turbulent boundary layer with a fluttering panel using direct numerical simulation. Phys. Fluids (2013). doi:10.1063/1.4819350
11. Vaicaitis, R., Dowell, E.H., Ventres, C.S.: Nonlinear panel response by a Monte Carlo approach. AIAA J. **12**(5), 685–691 (1974). doi:10.2514/3.49320
12. Abdel-Motagaly, K., Duan, B., Mei, C.: Nonlinear response of composite panels under combined acoustic excitation and aerodynamic pressure. AIAA J. **38**(9), 1534–1542 (2000). doi:10.2514/2.1175
13. Ibrahim, H.H., Tawfik, M., Negm, H.M.: Aerothermoacoustic response of shape memory alloy hybrid composite panels. J. Aircraft **46**(5), 1544–1555 (2009). doi:10.2514/1.39214
14. Sinay, L.R., Reiss, E.L.: Perturbed panel flutter-A simple model. AIAA J. **19**(11), 1476–1483 (1981). doi:10.2514/3.7876
15. Wang, X., Yang, Z., Zhou, J.: Aeroelastic effect on aerothermoacoustic response of metallic panels in supersonic flow. Chin. J. Aeronaut. **29**(6), 1635–1648 (2016). doi:10.1016/j.cja.2016.10.003
16. Zhao, H., Cao, D.: Supersonic flutter of laminated composite panel in coupled multi-fields. Aerosp. Sci. Technol. **47**, 75–85 (2015). doi:10.1016/j.ast.2015.09.019
17. Dowell, E., Edwards, J., Strganac, T.: Nonlinear aeroelasticity. J. Aircraft **40**(5), 857–874 (2003). doi:10.2514/2.6876
18. Nayfeh, A.H., Chin, C., Mook, D.T.: Parametrically excited nonlinear two-degree-of-freedom systems with repeated natural frequencies. Shock Vib. **2**(1), 43–57 (1995). doi:10.3233/SAV-1995-2105
19. O'Neil, T., Gilliatt, H., Strganac, T.: Investigations of aeroelastic response for a system with continuous structural nonlinearities. In: 37th structure, structural dynamics and materials conference. American Institute of Aeronautics and Astronautics (1996)
20. Gilliatt, H., Strganac, T., Kurdila, A.: Nonlinear aeroelastic response of an airfoil. In: 35th aerospace sciences meeting and exhibit (1997)
21. Kulikov, A.N.: 1:3 Resonance is a possible cause of nonlinear panel flutter. Comput. Math. Math. Phys. **51**(7), 1181–1193 (2011). doi:10.1134/S0965542511070128
22. Kulikov, A.N., Pilipenko, G.V.: Resonances in the problem of the panel flutter in a supersonic gas flow. Modelirovanie i Analiz Informatsionnykh Sistem [Model. Anal. Inf. Syst.] **18**(1), 56–67 (2011)
23. Zhu, W.Q., Lu, M.Q., Wu, Q.T.: Stochastic jump and bifurcation of a Duffing oscillator under narrow-band excitation. J. Sound Vib. **165**(2), 285–304 (1993). doi:10.1006/jsvi.1993.1258
24. Mantari, J.L., Oktem, A.S., Soares, C.G.: A new higher order shear deformation theory for sandwich and composite laminated plates. Compos. Part B Eng. **43**(3), 1489–1499 (2012). doi:10.1016/j.compositesb.2011.07.017
25. Tessler, A., Hughes, T.J.R.: A three-node Mindlin plate element with improved transverse shear. Comput. Method Appl Mech. Eng. **50**(1), 71–101 (1985). doi:10.1016/0045-7825(85)90114-8
26. Dowell, E.H.: Panel flutter-A review of the aeroelastic stability of plates and shells. AIAA J. **8**(3), 385–399 (1970). doi:10.2514/3.5680
27. Tian, W., Yang, Z., Gu, Y.: Analysis of nonlinear aeroelastic characteristics of a trapezoidal wing in hypersonic flow. Nonlinear Dyn. (2017). doi:10.1007/s11071-017-3511-4
28. Zhou, R.C., Xue, D.Y., Mei, C.: Finite element time domain-modal formulation for nonlinear flutter of composite panels. AIAA J. **32**(10), 2044–2052 (1994). doi:10.2514/3.12250
29. Ibrahim, R.A., Orono, P.O., Madaboosi, S.R.: Stochastic flutter of a panel subjected to random in-plane forces. I-Two mode interaction. AIAA J. **28**(4), 694–702 (1990). doi:10.2514/3.10448
30. Guo, X., Mei, C.: Application of aeroelastic modes on nonlinear supersonic panel flutter at elevated temperatures. Comput. Struct. **84**, 1619–1628 (2006). doi:10.1016/j.compstruc.2006.01.041
31. Sohn, K.J., Kim, J.H.: Nonlinear thermal flutter of functionally graded panels under a supersonic flow. Compos. Struct. **88**(3), 380–387 (2009). doi:10.1016/j.compstruct.2008.04.016